In press, High Temperature Corrosion and Protection of Materials 5 (2000), Les Embiez

Effects of Platinum Additions on the Adherence of Alumina Scales to CVD Aluminide Bond Coatings

J.A. Haynes[1], K.L. More,[1] B.A. Pint[1], I.G. Wright[1], K. Cooley[1], Y. Zhang[1,2]

[1]Oak Ridge National Laboratory, P.O. Box 2008 Oak Ridge, TN, 37831-6063, USA
[2]Walbar Metals, Peabody, MA, 01961-3369 USA

Keywords: Bond coatings, TBC, platinum, aluminides, oxidation, CVD, hafnium

Abstract: It is well known that Al_2O_3 scale adherence to aluminide bond coats is enhanced by Pt alloying additions, however, the actual mechanisms of the Pt effect are not defined. Both NiAl and NiPtAl bond coats were fabricated on two types of single-crystal superalloys (de-sulfurized and nominal S content) by a high-purity chemical vapor deposition (CVD) process. Oxide scale adherence to CVD NiAl during thermal cycle testing to 1150ºC was dramatically improved by reducing both superalloy and coating S impurities. Platinum additions to CVD aluminides resulted in significant further improvements in scale adherence, especially on the higher-S superalloy. The most obvious manifestation of the Pt effect was elimination of large voids at the oxide-metal interface. Transmission electron microscopy of α-Al_2O_3 scales after isothermal exposure indicated internal void growth on both NiAl and NiPtAl, but scales on NiPtAl also contained Hf from the superalloy. These results further support previous observations that Pt mitigates the detrimental effect of S impurities by modifying the driving force to stabilize or accelerate void growth, although this may not be the only beneficial effect.

1. INTRODUCTION

There is significant interest in developing oxidation-resistant (Al_2O_3-forming) metallic coatings that can effectively operate at very high combustion temperatures, and whose performance characteristics delay the first oxide scale spallation event as long as possible. Such coatings are intended for use as bond coats in state-of-the-art thermal barrier coating (TBC) systems, where the failure mode is spallation of the ceramic top coat due to failure of the Al_2O_3 scale that forms along the bond coat-top coat interface [1,2]. Recently, single-phase platinum aluminide coatings fabricated by a high-temperature, low activity chemical vapor deposition (CVD) aluminizing process [3] have become widely accepted as a bond coating for higher-temperature TBC applications.

Currently, there are three well-established methods of improving Al_2O_3 scale adherence; (1) addition of a reactive element (RE), such as Y, Hf, or Zr [4, 5], (2) alloying with precious metals (Pt, Pd, or Ir) [6], and (3) reduction of S impurities [7,8]. Proper addition of a RE to aluminide coatings is not yet feasible due to manufacturing limitations. The oxidation performance of commercial aluminide coatings has been enhanced by Pt additions for over 20 years [9], but the mechanism has not been explained and, thus, it is difficult to devise methods to optimize the Pt benefit or even to define its limitations. Most investigations of S impurity effects have primarily focused on un-coated superalloys [10], but there is also significant need to understand the influence of S impurities on aluminide bond coat oxidation behavior.

Previous work in this laboratory demonstrated that reduction of S impurity levels in both the superalloy substrate and the overlying CVD NiAl coating enhanced Al_2O_3 scale adherence [11]. Platinum additions to the coatings provided significant further improvements in oxide adherence, even though the electroplated Pt contained high levels of S [12]. This observation led to the realization that, in Pt-modified coatings, the detrimental influence of S is mitigated by a mechanism that has not been previously identified. Based on microstructural observations from isothermal oxidation studies of NiAl and NiPtAl coatings on low-sulfur superalloys, it was concluded that for certain S levels the presence of Pt can suppress or eliminate void growth at the oxide-metal interface, likely by altering the driving force(s) by which S impurities stabilize and/or accelerate void growth [13]**.** In order to gain an improved understanding of this phenomenon, the present study focused on evaluation of the isothermal and cyclic oxidation behavior of CVD NiPtAl coatings on superalloys with higher sulfur levels, as well as characterization and comparison of oxide scales formed on CVD NiAl and NiPtAl coatings.

2. EXPERIMENTAL

Two Y-free versions of René N5, a second-generation, single-crystal (SX) superalloy (Table 1) were used as substrates in this study. One alloy was melt de-sulfurized and the other was of nominal S content. Glow-discharge mass spectroscopy (GDMS) indicated a bulk S content of ~0.4 ppmw for the low-S (LS) superalloy and ~ 3 ppmw for the high-S (HS) alloy. Substrates (1.8 cm x 1.4 cm x 0.15 cm coupons or 1.65 cm diameter x 0.159 cm discs) were polished on all surfaces prior to aluminizing. As described previously [11], low-sulfur NiAl coatings were fabricated by a conventional, low Al-activity CVD aluminizing procedure using a reactor specifically modified to minimize process-related S contamination. The NiPtAl coatings were synthesized by first electroplating the substrates with ~7 μm Pt and then aluminizing by the identical CVD procedure [12]. As-deposited CVD NiAl- and NiPtAl-coated specimens on LS and HS substrates were tested by cyclic (1-h cycles) and isothermal oxidation at 1150°C. Surfaces and cross-sections of coatings and oxide scales were examined by field-emission gun-scanning electron microscopy (FEG-SEM). Oxide scales on selected specimens were examined by scanning transmission electron microscopy with energy dispersive spectroscopy (STEM/EDS). The TEM foils were prepared by a focused ion beam (FIB) technique, which allowed preparation and examination of the entire scale cross-section [15].

Table I. Composition of Single-Crystal René N5 Substrates (Y-free)

Element	Ni	Co	Cr	Ta	Al	W	Re	Mo	Hf	Ti	C
Wt%	63.38	7.33	7.03	6.42	6.05	5.13	3.05	1.40	0.15	0.01	0.05
At%	64.92	7.48	8.13	2.13	13.48	1.68	0.99	0.88	0.05	0.01	0.25

3. RESULTS AND DISCUSSION

3.1 As-fabricated Coatings

The as-fabricated CVD NiAl and NiPtAl coatings are described in detail elsewhere [11-13]. The coating surfaces consisted of a network of grain boundaries (20 – 150 μm grain diameters) with prominent ridges (Fig. 1a). Both coatings consisted of a columnar-grained, single-phase (β-NiAl or β-NiPtAl) surface layer (25 to 40 μm thick) over a complex interdiffusion zone (Fig. 1b).

3.2 Cyclic Oxidation Behavior

The cyclic oxidation behavior of the simple aluminide coatings was very sensitive to substrate S impurity levels. Figure 2 compares the specific weight gains as a function of number of cycles for

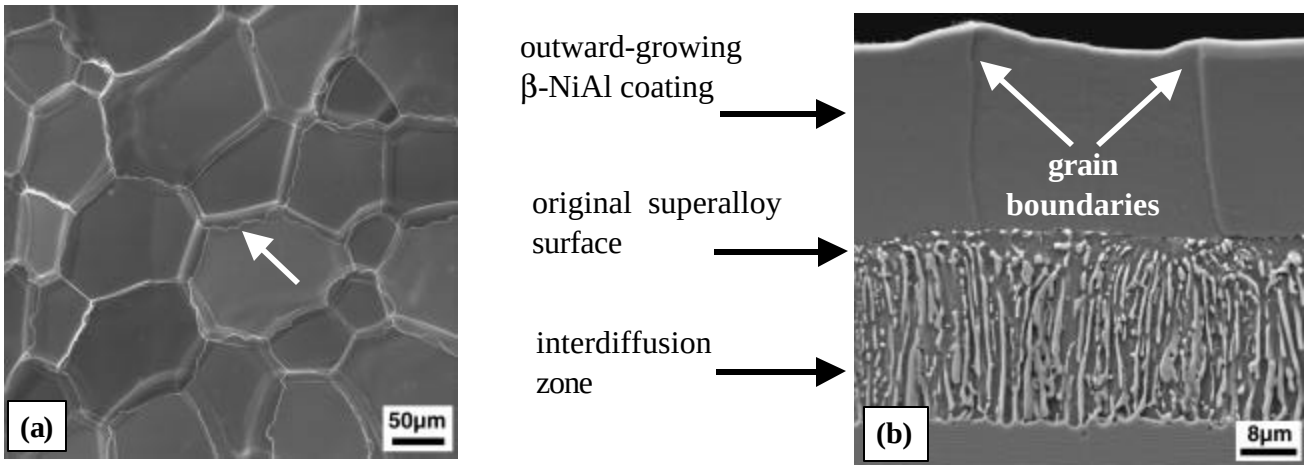

Fig. 1. SEM images of as-fabricated coatings. (a) Surface of as-deposited CVD NiPtAl, and (b) etched cross-section of CVD NiAl, showing the typical columnar grain structure and surface ridges.

representative CVD NiAl and CVD NiPtAl coatings on both HS and LS René N5. The CVD NiAl on HS substrates experienced massive Al_2O_3 scale spallation at approximately 40 cycles, as indicated by mass loss (Fig. 2). By comparison, Al_2O_3 scales on CVD NiAl + LS René N5 exhibited excellent adherence for a simple aluminide, but began to experience measurable amounts of oxide spallation after ~200 cycles (Fig. 2). Most scale damage on LS NiAl occurred along the surfaces of the aluminide grain boundary ridges, and initiated prior to 100 cycles (Fig. 3a). Although the bulk NiAl grains contained adherent Al_2O_3 after 200 cycles, previous investigations revealed that the NiAl coating grain boundaries had transformed to γ'-Ni_3Al, which has much poorer scale adherence than β-NiAl [13].

In contrast to the simple aluminides, the oxidation behavior of the Pt-modified coatings was not influenced by the S content of the substrates. In general, the oxidation performance of NiPtAl was very similar on both HS and LS René N5 within the time frame of these tests (Fig. 2). Comparison of scale adherence on NiPtAl + HS René N5 to that of NiAl + LS René N5 in Figs. 3(a) and (b) after 100 cycles illustrates the minimal influence of S content on the oxidation performance of Pt-modified coatings. The NiPtAl exhibited no scale damage (Fig. 3b), even though the substrate contained relatively high S concentrations. Localized cracking of Al_2O_3 scales on the grain boundary ridges (with occasional spallation and exposure of bare metal) was common on NiAl after 100 cycles, even though S levels were significantly lower (Fig 3a). The duration of the Pt effect is illustrated in Figs. 4(a) – (d), which compare the surfaces of CVD NiPtAl coatings on LS and HS René N5 after 700 cycles. Both coating surfaces experienced similar amounts of localized oxide cracking (primarily along grain boundary ridges), minor amounts of oxide spallation, and noticeable amounts of surface deformation. Approximately 99% of both coating surfaces contained adherent scale after 700 cycles, although there was clear evidence that moderate amounts of localized scale spallation and re-formation had occurred on both Pt-modified coatings (Fig. 4c and d), as suggested by Fig. 2.

3.3 Isothermal Oxidation Behavior of Coatings on Low-sulfur Substrates

Alumina scale adherence to β-NiAl is typically compromised by extensive void formation at the oxide-metal interface [16]. Isothermal oxidation testing is particularly advantageous for evaluating void growth behavior, since it involves a single cooling cycle, typically after a long exposure. In this case void formation is not masked by repeated scale spallation and re-formation during thermal cycling.

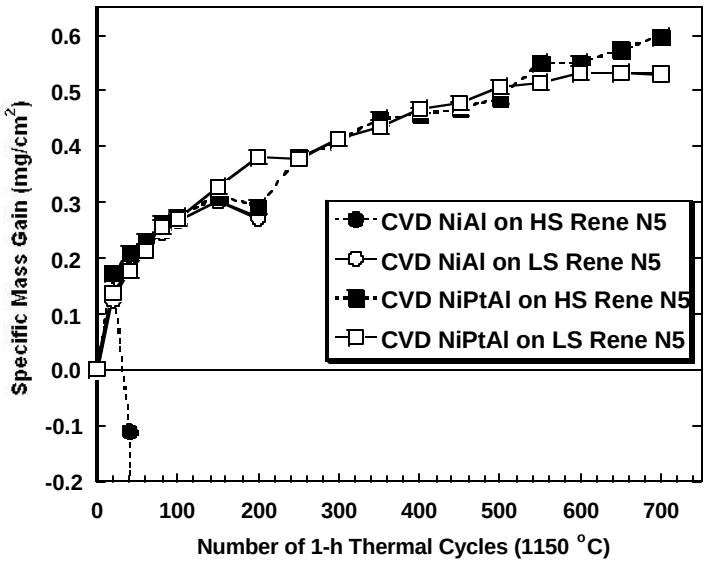

Fig. 2. Representative cyclic oxidation mass gains (1-h cycles, 1150ºC), comparing the scale adherence of CVD NiAl and NiPtAl on high-sulfur and low-sulfur René N5 superalloy substrates.

Microstructural observations after isothermal oxidation testing of CVD NiAl + LS René N5 at 1150ºC revealed time-dependent growth of large (1 – 30 μm) voids at the oxide-metal interface, as discussed previously [13,14]. These rapid-growing voids typically formed over the columnar NiAl grain boundaries (Fig. 5a). In contrast, no oxide-metal voids were observed in cross-sections of NiPtAl + LS René N5 after 200-h isothermal oxidation [13,14]. Additionally, thermogravimetric analysis revealed measurably slower growth kinetics for oxide scales on CVD NiAl ($k_p = 7.0 \times 10^{-14}$ $g^2cm^{-4}s^{-1}$) as compared to those on CVD NiPtAl ($k_p = 1.4 \times 10^{-13}$ $g^2cm^{-4}s^{-1}$). The difference in kinetics was confirmed by metallographic comparison of scale thickness [14]. Metallographic observations of etched CVD NiAl by FEG-SEM also revealed fine (<100 nm) bright-contrast particles non-uniformly distributed along the oxide-metal interface (Fig. 5b). A uniform dispersion of very fine spherical particles (~10 nm) was also observed in the β-NiAl matrix (Fig. 5b). These precipitates were also present in NiPtAl and were identified as α-Cr particles, as will be discussed in a subsequent section.

3.4 Isothermal Oxidation Behavior of Coatings on High-sulfur Substrates

CVD NiAl and NiPtAl on HS René N5 were exposed to 200-h isothermal oxidation at 1150ºC to further investigate the influences of Pt on void growth. It was postulated that void growth would be slowed or prevented in the Pt-modified coating, whereas void growth would be extensive on the simple aluminide due to the relatively high S content of the substrate. This theory was confirmed, as practically every grain boundary on the CVD NiAl surface contained numerous large-diameter voids, whereas no Al_2O_3 spallation was observed on NiPtAl (Fig. 6b). Voids on NiAl often elongated into grain boundary trenches (Fig. 6a) and the bulk surfaces of many grains also contained numerous voids. Approximately 40% of the scale spalled from the NiAl during the single cooling cycle (Fig. 6a).

3.5 TEM Characterization of Oxide Scales on Low-sulfur Coatings

Preliminary analyses of oxide scales on CVD NiAl and NiPtAl coatings on LS René N5 were conducted by TEM and STEM/EDS after 100-h isothermal oxidation (1150ºC). Figures 7(a) and (b) compare scale microstructures and flaw contents on single grains of NiAl and NiPtAl, respectively. The α-Al_2O_3 scales on NiAl (Fig. 5 is from the same specimen) were one grain thick and appeared

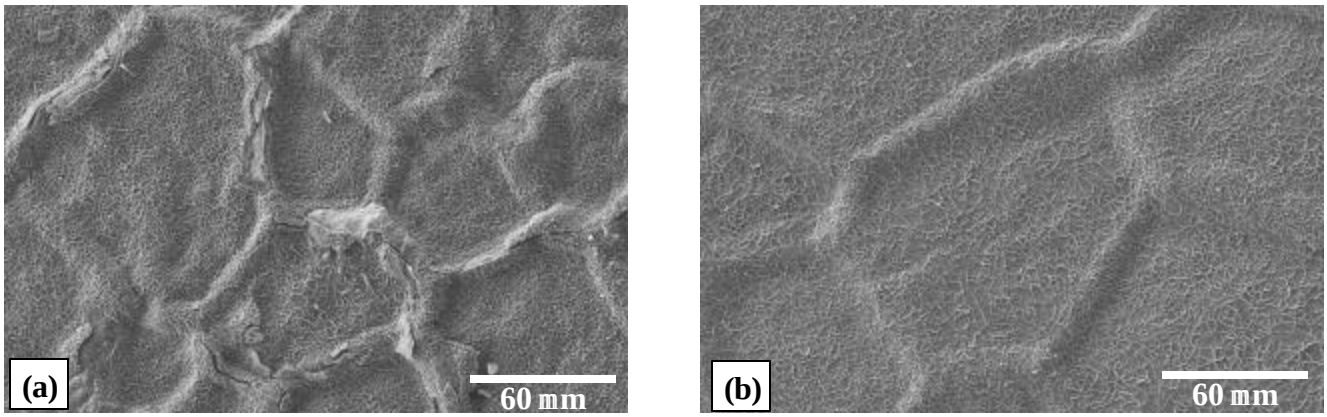

Figure 3. SEM images of oxidized coating surfaces after 100, 1-h cycles to 1150ºC.. (a) CVD NiAl (no Pt) on low-S René N5, with cracked grain boundary scales, and minor amounts of localized Al_2O_3 spallation, (b) CVD NiPtAl on high-S René N5, with no Al_2O_3 cracking or spallation.

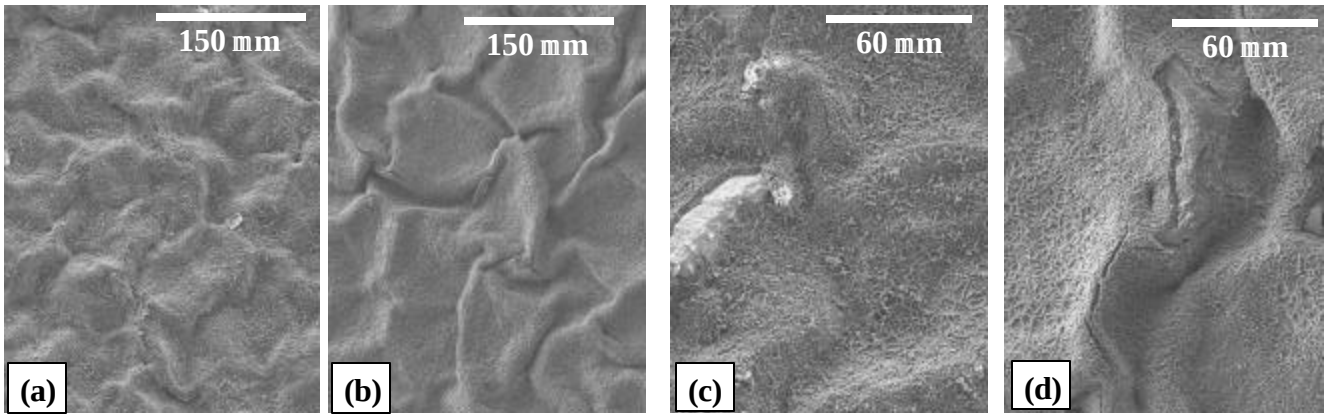

Fig. 4. SEM images of oxidized CVD NiPtAl coating surfaces after 700 1-h cycles to 1150ºC. (a), (c) Coatings on low-S René N5. (b), (d) Coatings on high-S René N5. Both exhibited very similar characteristics (i.e., scales on grain boundaries were often cracked, but little bare metal was exposed).

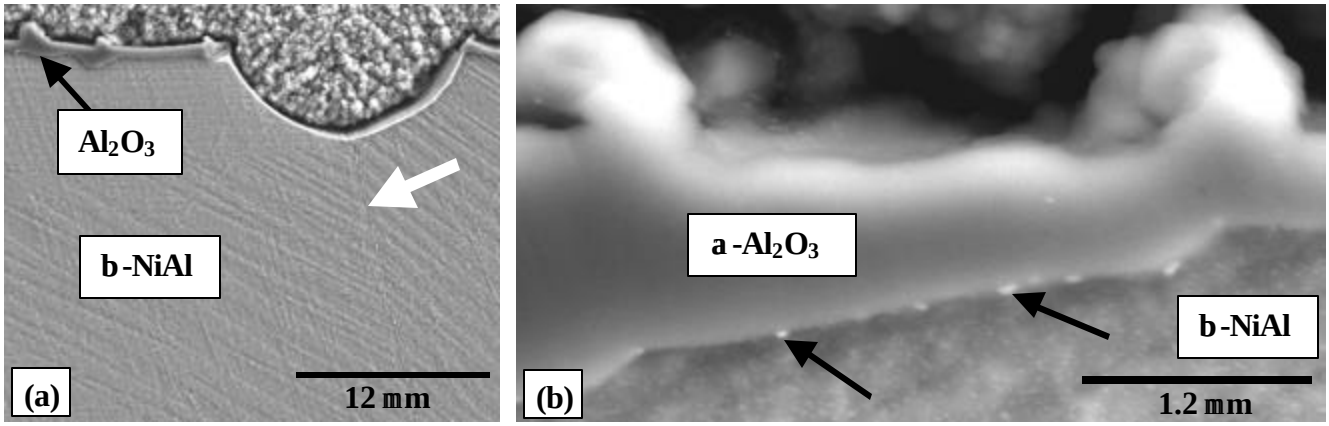

Fig. 5. SEM images of CVD NiAl on LS René N5 after isothermal oxidation (100h, 1150ºC). (a) Typical void formed over NiAl grain boundary (large arrow). (b) Oxide-metal interface containing bright-contrast particles (arrows) with very fine spherical particles in the β-NiAl.

equiaxed in morphology (Fig. 7a), as would be expected for scales not doped with a RE. The scales ranged from 0.4 – 1.5 μm in thickness, with an average thickness of ~1.1 μm and a grain diameter of ~2.0 μm. The large Al_2O_3 grain size may partially explain the unexpectedly slow scale growth rates on NiAl, if scale growth was primarily controlled by O and Al grain boundary diffusion (assuming no doping by substrate Hf, as discussed below). High concentrations of fine internal voids (<100 nm) were distributed throughout the scale thickness, but there were no voids at the oxide-metal interface.

There were significant differences in the microstructures of Al_2O_3 scales on CVD NiPtAl, as compared to NiAl. Scales on NiPtAl were measurably thicker (1 – 2.5 μm) and appeared to consist of two discrete layers (Fig. 7b). The larger-grained outer layer was similar to the scales on NiAl. It appeared equiaxed, with an irregular external surface and a significant concentration of internal voids (i.e., Pt addition did not prevent internal void formation in Al_2O_3), although the void concentration was less than was observed for scales on NiAl. This outer layer was ~1.2 μm thick with a grain diameter of ~1.3 μm. The inner layer consisted of finer-grained Al_2O_3 (~0.6 μm) having a thickness of ~1.0 μm with the appearance of a columnar microstructure, similar to those encountered in RE-doped scales. The columnar-grained inner layer of Al_2O_3 contained no internal voids (Fig 7b). These observations led to the expectation that the columnar region of scale was doped with Hf, which was present at a concentration of ~0.05 at.% in the superalloy substrate (Table 1).

Elemental mapping of oxide scales on NiPtAl by STEM/EDS confirmed the presence of Hf at the oxide-metal interface and along the columnar Al_2O_3 grain boundaries (Fig. 8a). No Hf was detected in the oxide on NiAl (Fig. 7a). These results suggest that Hf diffusion rates or solubility may be higher in NiPtAl. Since Hf is known to decrease alumina growth rates by up to an order of magnitude [17], the lower scale growth kinetics on NiAl were unexpected. As mentioned previously, the slower growth rates may have been due to the larger Al_2O_3 grain size on NiAl. Alternatively, it may be related to a slower transition from the faster-growing transient θ-alumina to the slower-growing α-alumina on the Pt-containing surfaces, as suggested by other authors [18]. Since the present TEM results are from a single NiPtAl grain, the uniformity of Hf-doping is uncertain. Additional TEM studies are being conducted in order to further evaluate Hf segregation. It is not clear whether proximity of the scale to a coating grain boundary influences Hf content, since Hf diffusion along the columnar aluminide grain boundaries (Fig. 1b) would be much more rapid than bulk diffusion. Aluminide grain orientation may also play a role in modifying Hf diffusion rates or oxide phase transformations. It should be noted that

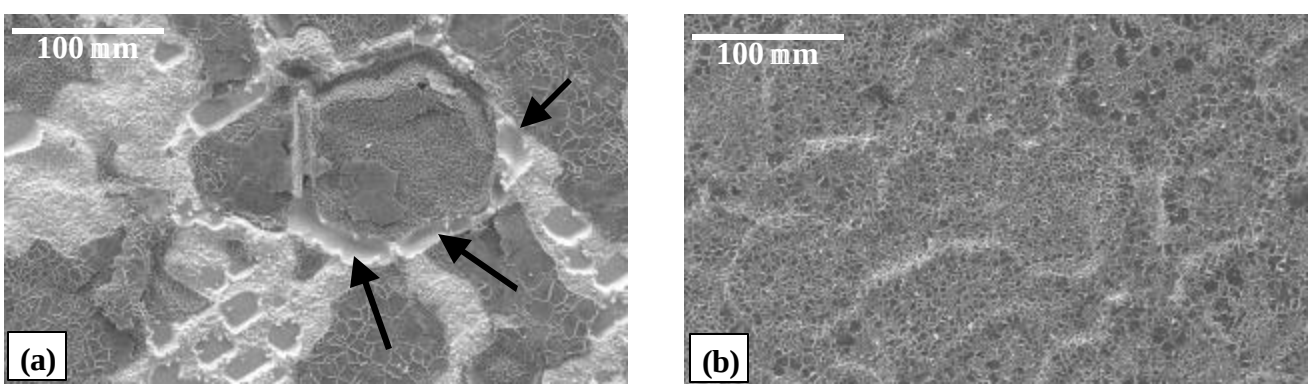

Fig. 6. SEM surface images of coatings on high-S René N5 after isothermal oxidation (200-h, 1150ºC). (a) CVD NiAl. Note the extensive scale spallation and numerous voids on the surface, especially along NiAl grain boundaries (arrows). (b) No scale spallation or voids were observed on CVD NiPtAl.

the good scale adherence to NiPtAl cannot necessarily be attributed to Hf, since no Hf was detected in the outer layer of scale by STEM/EDS. Apparently, Hf diffused through the coating during oxidation and eventually reached sufficient concentration at the oxide-metal interface to activate the RE effect, where the primary scale growth mechanism is inward grain boundary diffusion of oxygen [4].

Further examination by STEM/EDS and electron diffraction revealed numerous α-Cr particles at the oxide-metal interface and in the β-phase matrix of both CVD NiAl and NiPtAl. The EDS maps in Figs. 8b and c show the location and morphology of these particles, which coincide with the SEM observations of Fig. 5b. The maps also reveal that these Cr-rich particles contain Re and Co (not shown). The interface particles were larger (~100 nm) and were typically elongated along the oxide-metal interface (Fig. 8b and c). The spherical α-Cr particles were approximately 10 nm in diameter and were uniformly distributed throughout the coating (Fig. 8b), indicating low solubility of Cr, Re and Co in the β- phase. This finding is significant since the presence of the α-Cr particles (with significantly lower coefficient of thermal expansion than β-NiAl) at the oxide-metal interface may impose additional interface strain during thermal cycling. However, these particles clearly did not result in rapid scale failure or void formation on NiPtAl, although prior results do suggest that addition of Cr can reduce long-term scale adherence to aluminides [17].

4.0 SUMMARY

Comparison of the isothermal and cyclic oxidation behavior (i.e., void formation and scale adherence) of CVD NiAl and NiPtAl coatings on identical high-S and low-S superalloy substrates has more rigorously demonstrated the capability of Pt to reduce or eliminate the detrimental influence of S impurities. Specifically, void formation was eliminated in Pt-modified coatings. Preliminary analysis of oxide scales by TEM and STEM/EDS revealed thin, large-grained Al_2O_3 with no detectable Hf on CVD NiAl. Scales on CVD NiPtAl were thicker and contained a columnar-grained inner layer of Al_2O_3 doped with Hf. It is possible that Pt enhances the RE effect by altering Hf diffusion behavior.

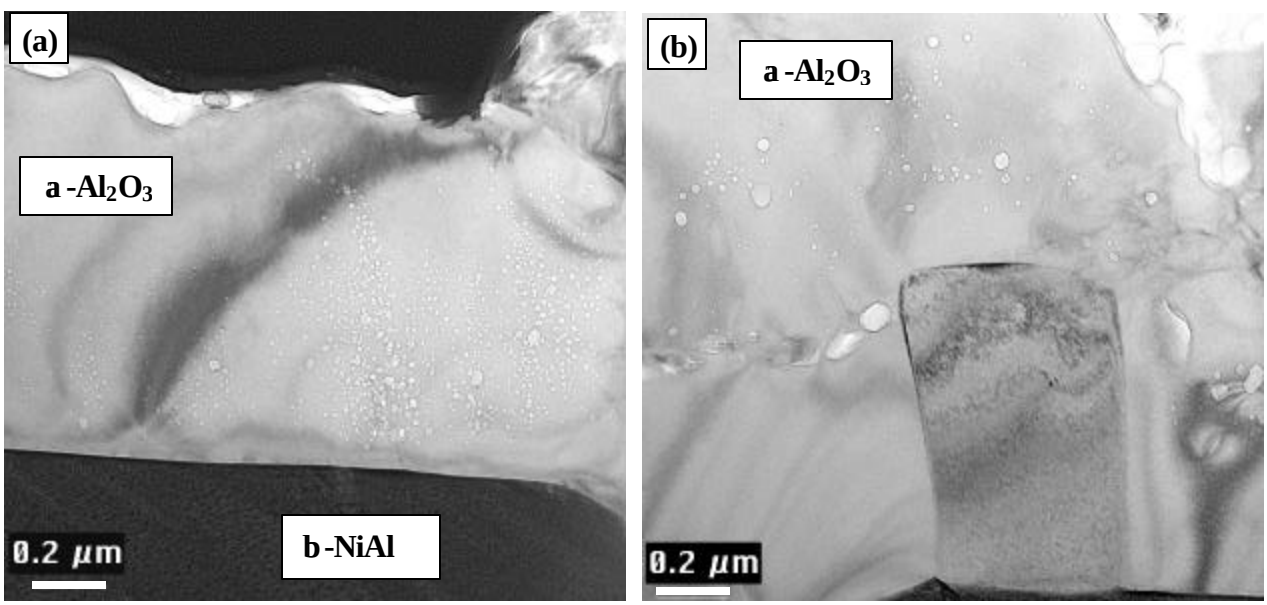

Fig. 7. TEM cross-section views of α-Al_2O_3 scales after isothermal oxidation (100h, 1150ºC) of coatings on low-sulfur René N5. (a) Scale on CVD NiAl. (b) Scale on CVD NiPtAl.

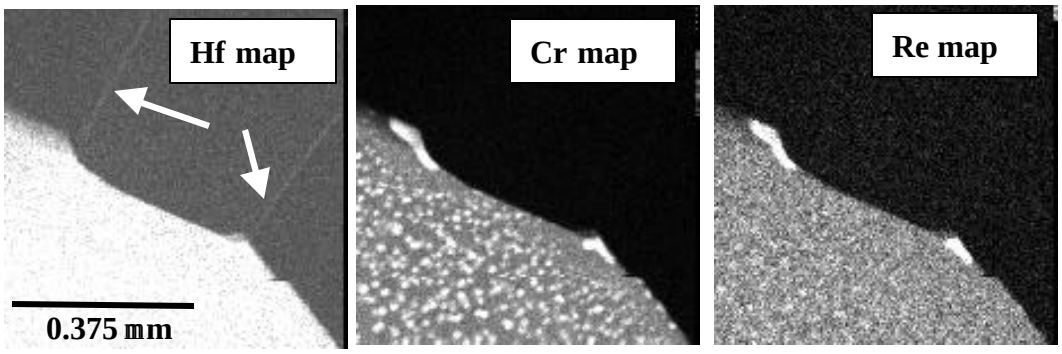

Fig. 8. STEM/EDS maps of (a) Hf, (b) Cr and (c) Re, at the alumina-metal interface on NiPtAl after 100-h oxidation (at 1150ºC). Hf was detected at the interface and the Al_2O_3 grain boundaries (arrows).

5. ACKNOWLEDGMENTS

The authors thank L.D. Chitwood, G. Garner and T. Geer at ORNL for assisting with the oxidation experiments and metallography, and P. Tortorelli and M. Lance at ORNL for reviewing the manuscript. Research sponsored by the U.S. Department of Energy, Assistant Secretary for Energy Efficiency and Renewable Energy, Office of Industrial Technologies, Advanced Turbine Systems Materials Program, under contract DE-AC05-96OR22464 with Lockheed Martin Energy Research Corporation.

6. REFERENCES

1. MEIER S.M., GUPTA D.K., SHEFFLER K.D., JOM, 43 (1991) 50-53
2. MARICOCHI A., BARTZ A., WORTMAN D.J., J. Thermal Spray Technol. 6 (2) (1997) 193-198
3. WARNES B.M., PUNOLA D.C., Surf. Coat. Technol., 94-95(1997) 1-6
4. PINT B.A., Oxid. Met. , 45 (1996) 1-37
5. STRAWBRIDGE A., HOU P.Y., Mater. High Temps., 12 (1994) 177-81
6. FELTEN E.J., PETTIT F.S., Oxid. Met., 10 (1976) 189-223
7. SMEGGIL J.G., FUNKENBUSCH A.W., BORNSTEIN N.S., Metall. Trans. A, 17A (1986) 923-932
8. SMIALEK J.L., Metall. Trans. A, 18A (1987) 164-167
9. FARRELL M.S., BOONE D.H., STREIFF, R., Surf. Coat. Technol.,32 (1987) 69-84
10. SMIALEK J.L., JAYNE D.T., SCHAEFFER J.C., MURPHY W.H., Thin Solid Films 253 (1994) 285-29
11. LEE W.Y., ZHANG Y., WRIGHT I., PINT B.A., LIAW P., Metall. Trans. A, 29A (1998) 833-841
12. ZHANG Y., LEE W. Y., HAYNES J.A., WRIGHT I. G., PINT B. A., COOLEY K. M., LIAW P. K., Met. Trans. A, 30A, (1999) 2679 – 2687
13. HAYNES J.A., ZHANG Y., LEE W.Y., PINT B.A., WRIGHT I.G., COOLEY, K.M., Elevated Temperature Coatings: Science and Technology III, J.M. Hampikian and N.B. Dahotre, Eds., (The Minerals, Metals and Materials Society, 1999) pp.185-196
14. ZHANG Y., HAYNES J.A., LEE W.Y., WRIGHT I.G., PINT B.A., submitted to Metall. Trans. A
15. PINT B.A., MORE K.L, WRIGHT I.G., TORTORELLI P.F., to be published in Microscopy of Oxidation 4, S.B. Newcombe and J.A. Little (Eds.), 2000
16. BRUMM M.W., GRABKE H.J., Corr. Sci., 34 (1993) 547- 553
17. PINT B.A., HAYNES J.A., MORE K.L, WRIGHT I.G., LEYENS C., subm. to Superalloys 2000
18. ROUX J.P., BRUMM M.W., GRABKE H.J., Fresnius J. Anal. Chem., 346 (1993) 265-268